J Toxicol Pathol 2025; 38: 69–82

Original Article

Identification and characterization of spontaneous AA amyloidosis in CD-1 mice used in toxicity studies: implications of SAA1 and SAA2 copy number variations

Mao Mizukawa[1,2*], Kohei Tanaka[3], Akane Kashimura[1], Yu Uchida[2], Takanori Shiga[2], Naoyuki Aihara[2], and Junichi Kamiie[2*]

[1] Safety Research Laboratories, Research Division, Mitsubishi Tanabe Pharma Corporation, Shonan Health Innovation Park, 2-26-1 Muraoka-Higashi, Fujisawa-shi, Kanagawa 251-8555, Japan
[2] Laboratory of Veterinary Pathology, School of Veterinary Medicine, Azabu University, 1-17-71 Fuchinobe, Chuo-ku, Sagamihara-shi, Kanagawa 252-5201, Japan
[3] DMPK Research Laboratories, Research Division, Mitsubishi Tanabe Pharma Corporation, 1000 Kamoshida-cho, Aoba-ku, Yokohama-shi, Kanagawa 227-0033, Japan

Abstract: Amyloidosis is characterized by the extracellular deposition of insoluble protein fibrils that cause cellular damage and dysfunction in organs and tissues. Multiple types of amyloidosis and their causative precursor proteins have been identified in humans and animals. In toxicological studies, a high incidence of spontaneous amyloidosis has been reported in CD-1 mice; however, the precursor protein responsible remains unclear. In contrast, B6C3F1 mice have a low incidence of amyloidosis. This study aimed to identify the types of amyloidosis and causative precursor proteins in CD-1 mice and investigate the role of copy number variations (CNVs) in genes encoding precursor proteins in different mouse species. Histopathological examination revealed amyloids in multiple organs, which were confirmed by direct fast scarlet staining. Immunohistochemistry and liquid chromatography-tandem mass spectrometry analyses revealed that the deposition was derived from serum amyloid A (SAA1 and 2), suggesting that the CD-1 mice had AA amyloidosis. Copy number variation assays demonstrated higher copy numbers of SAA1 and SAA2 in CD-1 mice with amyloidosis than in C3H/He mice (the parent strain of B6C3F1 mice). These findings suggest that the high copy numbers of SAA1 and SAA2 may contribute to the high incidence of AA amyloidosis in CD-1 mice. This study examined spontaneous amyloidosis in CD-1 mice and revealed the correlation between SAA1 and SAA2 CNVs in the pathogenesis of the disease and the genetic factors influencing amyloidosis in mice.
(DOI: 10.1293/tox.2024-0070; J Toxicol Pathol 2025; 38: 69–82)

Key words: CD-1 mice, amyloidosis, AA amyloidosis, serum amyloid A (SAA), copy number variation (CNVs)

Introduction

Amyloidosis is characterized by the extracellular deposition of insoluble protein fibrils in various organs and tissues. Local or systemic deposition of amyloid fibrils causes cellular damage and dysfunction in the affected tissues or organs[1, 2]. Amyloidosis is defined based on the precursor protein. Thirty-six types of amyloid fibrils have been identified in humans, 11 of which have been identified in various animal species[1]. In mice, systemic amyloidosis is known as an age-related disease. C57BL6/J mice[3] and other strains[4, 5] have been reported to develop spontaneous apolipoprotein A-II (ApoA2) amyloidosis. Additionally, experimental induction of AA amyloidosis has been reported in mice, in which amyloidosis occurs secondary to inflammation, such as subcutaneous inflammation, induced by the administration of stimuli (e.g., $AgNO_3$) or intravenous administration of amyloid enhancing factor[6, 7]. In long-term general toxicity or carcinogenicity studies conducted for the development of pharmaceuticals and testing of pesticides, spontaneous systemic amyloidosis in the liver, spleen, kidney, gastrointestinal tract, and adrenal glands was observed in CD-1 mice[8, 9]. Amyloidosis is one of the causes mortality in CD-1 mice[8]. Furthermore, the incidence of amyloidosis in CD-1 mice has been reported to be higher than that in B6C3F1 mice, which are a cross between C57/BL6 and C3H mice[9]. In these toxicity studies, amyloidosis or amyloid deposits were usually diagnosed in hematoxylin and eosin (HE)-stained specimens

Received: 6 August 2024, Accepted: 26 October 2024
Published online in J-STAGE: 13 November 2024
*Corresponding authors:
M Mizukawa (e-mail: mizukawa.mao@ma.mt-pharma.co.jp);
J Kamiie (e-mail: kamiie@azabu-u.ac.jp)
(Supplementary material: refer to J-STAGE https://www.jstage.jst.go.jp/browse/tox)

without special staining, such as with direct fast scarlet (DFS) or Congo red. Moreover, no additional analyses, such as immunohistochemistry or proteomics, were conducted to identify the amyloid types or precursor proteins. Consequently, the type of spontaneous amyloidosis occurring in CD-1 mice remains unknown. This study aimed to identify the types of spontaneous amyloidosis and their precursor proteins in CD-1 mice. In the present study, we used organs and tissues from 16 CD-1 mice (Group 1: Crlj:CD1(ICR) and Group 2: Crl:CD1(ICR)) to conduct histopathological, immunohistochemical, and ultrastructural examinations, and liquid chromatography-tandem mass spectrometry (LC-MS/MS) analysis to identify and characterize the types of amyloidosis in these animals. In addition, given that copy number variations (CNVs) are associated with the duplication or depletion of genomic DNA in human disease[10, 11], we hypothesized that CNVs are associated with amyloidosis in CD-1 mice. We conducted real-time polymerase chain reaction (PCR) to investigate the copy numbers of genes encoding precursor proteins in CD-1 mice with and without amyloidosis, as well as in several mouse species.

Materials and Methods

Animals and sample collection

All samples used in the present study originated from each study site: Mitsubishi Tanabe Pharma Corporation (Kanagawa, Japan), BoZo Research Center Inc. (Shizuoka, Japan), or Azabu University (Kanagawa, Japan). The studies were approved by the Institutional Animal Care and Use Committee of the conducting site and all experiments involving animals were conducted in accordance with the guidelines of the Animal Care and Use of the institution.

Formalin-fixed paraffin-embedded (FFPE) blocks and formalin-fixed tissues samples from CD-1 mice with amyloidosis used in the present study were provided by the BoZo Research Center, Inc. The CD-1 mouse strains used were Crlj:CD1(ICR) and Crl:CD1(ICR), which are pre-(Crlj) or post-(Crl)-Institute for Genomic Standardizations (IGS). Formalin-fixed paraffin-embedded samples from CD-1 mice without amyloidosis and other mouse strains (C57/BL6J, C3H/HeN, DDY, and BALB/c) used for the CNV assay were originated from Mitsubishi Tanabe Pharma Corporation or Azabu University, as listed in Supplementary Table 1.

Histopathological examination

The characteristics of the mice used in this study are listed in Table 1. Organs and tissues in which deposition of amyloid-like substances was observed in HE-stained specimens were fixed in 10% formalin neutral buffer solution and embedded in paraffin. The paraffin-embedded samples were sectioned into 4 and 10 μm-thick sections that were stained with HE and DFS, respectively. Slides of HE-stained liver, kidney, spleen, heart, stomach, and duodenum samples were prepared for microscopic examination. Direct fast scarlet-stained sections were prepared for light and polarized microscopic examinations. Organs and tissues with DFS-positive staining were defined as having amyloidosis or amyloid deposits. To assess the severity of amyloid deposition, the liver, spleen, kidney, heart, and duodenum specimens were graded on a five-point scale as absent (−), minimal (±), mild (+), moderate (++), and severe (+++).

Immunohistochemistry

Organs and tissues with DFS-positive staining were selected for immunohistochemistry. The samples were deparaffinized and reacted with Mouse Serum Amyloid A1/A2 (SAA) antibody (R&D Systems, Minneapolis, MN, USA,

Table 1. Information on CD-1 Mice with Amyloidosis

Group no.	Case no.	Strain	Sex	Fate	Age (weeks)	Day*	Inflammatoly lesions	TEM
1	1	Crlj:CD-1(ICR)	Male	ME	83	540	Skin; Ulcerative dermatitis: +	-
	2	Crlj:CD-1(ICR)	Male	ME	88	577	Skin; Ulcerative dermatitis: +	-
	3	Crlj:CD-1(ICR)	Male	ME	82	532	Skin; Ulcerative dermatitis: +, Penis; Erosion/ulcer: +	-
	4	Crlj:CD-1(ICR)	Male	ME	101	671	Joint Knee; Arthritis: +	-
	5	Crlj:CD-1(ICR)	Male	ME	94	619	Skin; Ulcerative dermatitis: +	-
	6	Crlj:CD-1(ICR)	Female	ME	104	691	-	-
2	7	Crl:CD-1(ICR)	Male	FD	72	465	Skin; Infiltration, subcutis, mixed: ++	-
	8	Crl:CD-1(ICR)	Male	ME	83	540	Skin; Ulcerative dermatitis: ++	-
	9	Crl:CD-1(ICR)	Male	SE	84	548	Skin; Ulcerative dermatitis, Joint Knee; Arthritis: ++	Perfomed[a]
	10	Crl:CD-1(ICR)	Male	FD	59	372	Skin; Ulcerative dermatitis: ++	-
	11	Crl:CD-1(ICR)	Male	FD	59	372	Preputial gland; Inflammation/Abscess: ++	-
	12	Crl:CD-1(ICR)	Male	FD	60	382	Skin; Ulcerative dermatitis: ++	-
	13	Crl:CD-1(ICR)	Male	SE	84	547	Skin; Ulcerative dermatitis: ++	-
	14	Crl:CD-1(ICR)	Male	FD	47	291	-	Perfomed[b]
	15	Crl:CD-1(ICR)	Male	SE	84	551	Preputial gland; Inflammation/Abscess: ++	-
	16	Crl:CD-1(ICR)	Male	FD	85	554	Skin; Ulcerative dermatitis: ++	-

*Gestinational day (date of study start is the 1st day) of ME, FD, or SE. [a]Liver and kidney. [b]Kidney. FD: Found dead; ME: Moribund euthnasia; SE: Scheduled euthanasia; TEM: transmission electron microscopy.

Cat No. AF2948, 7.5 µg/mL). The samples were stained using an automated staining device (HISTOSTAINER 48A; Nichirei Biosciences Inc., Tokyo, Japan) according to the manufacturer's instructions. Sections were incubated at room temperature with primary and secondary antibodies for 1 h and 30 min, respectively. The immunoreactivity of the sections was detected and visualized using a peroxidase-diaminobenzidine (DAB) reaction (Peroxidase Stain DAB Kit [Brown Stain]; Nacalai Tesque, Kyoto, Japan) before hematoxylin counterstaining.

Ultrastructural examination

Formalin-fixed kidney and liver samples from two mice with amyloidosis based on DFS staining were selected for transmission electron microscopy (TEM) evaluation. Ultrathin sections were prepared according to the conventional method, and electron staining was performed using uranyl acetate and lead. Liver and kidney findings were evaluated using a transmission electron microscope (JEM1400; JEOL Ltd., Tokyo, Japan).

Proteomic analysis

Protein components were extracted from FFPE liver sections of CD-1 mice with amyloidosis and from 3 CD-1 mouse without amyloidosis. Briefly, 20 µm-thick sections were cut from FFPE liver tissues. The sections were dewaxed with hexane before 100% dimethyl sulfoxide (DMSO) was added and incubated at 37°C for 16 h followed by centrifuging at 15,000 × g for 10 min. The supernatant was collected[12] and dried using a speed vacuum (Cold trap; AS One, Osaka, Japan).

The dried sample was dissolved in 50 µL buffer containing 5% SDS and 50 mM NH_4HCO_3. The reduction reaction was performed with 5 mM TECP for 10 min at 37°C followed by the alkylation with 125 mM IAA for 30 min at 37°C. Digestion was performed using the SP3 method with trypsin and Lys-C mix (Promega, Madison, WI, USA). Tryptic peptides were desalted using an SDB column (GL-Tip SDB; GL-Science, Tokyo, Japan) and dried using a speed vacuum. The dried samples were dissolved in 0.1% trifluoroacetic acid and 5% DMSO and measured using an Evosep One LC system (Evosep, Odense, Denmark) coupled to a Q Exactive mass spectrometer (Thermo Fisher Scientific, Waltham, MA, USA). Peptides were separated using an EV1137 column (15 cm × 150 µm ID with 1.5 µm media, Evosep) following the 30 SPD protocol. The column temperature was maintained at 40°C, and the mobile phases were 0.1% acetic acid in LC/MS grade water (buffer A) and 0.1% acetic acid in acetonitrile (buffer B). The mass spectrometer was operated in the data-dependent acquisition mode, with the 10 most intense ions in each MS scan subjected to MS/MS with a full scan range of 400–800 m/z at a resolution of 35,000. The precursor ion selection width was kept at 1.6 m/z and fragmentation was achieved by higher energy collisional dissociation at a normalized collision energy (NCE) of 30%.

Protein identification and quantification

Protein identification and quantification were performed using PEAKS Studio (version 10.0; Bioinformatics Solutions, Inc., Waterloo, ON, Canada), which enables *de novo* sequencing. We used PEAKS PTM search for the identification of unspecified/variable modifications and PEAKS Q for the quantification of protein and peptides. The database used was the UniProt Swiss-Prot canonical database. Carbamidomethylation of cysteine was set as a fixed modification.

The mass tolerance was set at 10 ppm for precursor ions and 0.02 Da for the product ion. Strict trypsin and Lys-C specificity were applied and three missed cleavages were allowed. The identified spectra were validated using the Target Decoy PSM Validator as implemented in PEAKS Studio and filtered for 1% FDR. The detected SAA1 and SAA2 peptide fragments (ion intensity of each peptide >1E+04) were confirmed. Proteins with an ion intensity >1.0E+05, and thus, a sufficient detection level, were listed, to identify differences in the major proteins detected in CD-1 mice with and without amyloidosis.

Real-Time PCR and copy number assay

Genomic DNA was extracted from FFPE tissue samples using the ReliaPrep FREP gDNA Miniprep System (Promega). Information on the samples from each mouse is provided in Supplementary Table 1. Real-time PCR was performed using the PrimeTime® Gene Expression Master Mix (IDT DNA, Coralville, IA, USA) according to the manufacturer's protocol. The TaqMan™ Copy Number Reference assay, mouse, transferrin (Tfrc; Thermo Fisher Scientific) was used as a reference gene for real-time PCR and to calculate copy numbers. The sequences of the primers and TaqMan probe sets, as well as the reagents for real-time PCR of SAA1 and SAA2 are shown in Supplementary Figure 1. The total reaction volume was 20 µL. Real-time PCR was performed using the StepOne™ Real-Time PCR System (Applied Biosystems, Foster City, CA, USA) with triplicate reactions for each sample. The mean values of SAA1 and SAA2 expression were calculated as a ratio to that of Tfrc according to the ΔΔCT method. Copy number analysis was performed using Copy CopyCaller® Software v2.1 (Thermo Fisher Scientific). Synthetic gene samples were prepared to select the reference animals for copy number calculations. The copy numbers calculated from the synthetic gene samples, which had the same copy numbers as the target genes SAA1, SAA2, and Tfrc, were used to select reference animals for each copy number calculation. The reference animals selected for copy number analysis of SAA1 and SAA2 were animals No. I7 and No. I10, respectively.

Results

Histopathological examination

Histopathological examination, eosinophilic substances, amyloid-like deposition were observed in HE-specimens. Deposition was observed in the liver, spleen, kidneys,

heart, and duodenum. The locations of the eosinophilic substances in each tissue and their severity are summarized in Table 2. In the liver (Fig. 1A), minimal to mild deposition of eosinophilic substances was observed in the perivascular portal and central vein. Minimal to severe deposits were observed in the space of Disse. Hepatocyte atrophy was observed in the areas with severe deposits. In the spleen, mild to severe deposition was observed in the red pulp and marginal zones. In the animals with severe deposits, the red pulp and marginal zone were replaced with eosinophilic substances (Fig. 1B). In the kidney, mild to severe deposition was observed in the glomerulus, whereas minimal to severe deposition was observed in the tubular interstitium of the cortex, inner and outer medullae, and renal papilla (Fig. 1C, 1D). Minimal deposits were observed in perivascular and interstitial cardiomyocytes (Fig. 1D). Deposition was also observed in the lamina propria of the duodenum (Fig. 1E). Overall, the occurrence of eosinophilic substances was severe in CD-1 mice and was associated with cellular damage and dysfunction such as atrophy or replacement of normal tissues.

Direct fast scarlet staining of the tissue samples was performed to determine whether the observed eosinophilic substances were amyloids. Eosinophilic substances were observed in the liver, spleen, kidney, heart, and duodenum, appearing red under light microscopy (Fig. 2A–2F) and exhibiting apple-green or yellow/orange birefringence under polarized light (Fig. 2G–2K). Together, the histological findings and DFS staining results indicated that the eosinophilic substances were consistent with amyloidosis or amyloid deposits.

Ultrastructural examination

To further confirm that the extracellular deposition was that of amyloids, ultrastructural examination of tissue samples from two CD-1 mice that exhibited amyloidosis in the liver and kidney was performed. In ultrastructural examination, an amyloid is defined as fibrils, bundled, non-branching, relatively straight, approximately 7.5–10 nm in diameter, and variable in length[13]. In the liver, non-branching fibrils with a diameter of approximately 10 nm were observed in the space of Disses (Fig. 3A, 3B). In the kidney, a

Table 2. Histopathological Examination of Tissues from CD-1 Mice with Amyloidosis

Organ and tissues	Case no.	1	2	3	4	5	6	7	8	9	10	11	12	13	14	15	16
	Sex	M	M	M	M	M	F	M	M	M	M	M	M	M	M	M	M
Liver																	
Amyloidosis /Amyloid deposit																	
perivascular, portal area		+	+	+	+	+	+	+	+	+	+	+	+	+	+	+	+
space of disse, midzonal to central zone		+	+++	++	++	+	±	++	++	+	+++	+++	++	++	++	++	+++
Immunohistochemistry		P	P	P	P	P	P	P	P	P	P	P	P	P	P	P	P
Spleen																	
Amyloidosis /Amyloid deposit																	
red pulp and marginal zone		+	++	+	+	+	+	+++	+++	+++	+++	+++	+++	+++	+++	+++	+++
Immunohistochemistry		P	P	P	P	P	P	P	P	P	P	P	P	P	P	P	P
Kidney																	
Amyloidosis /Amyloid deposit																	
glomerulus		+	++	±	++	+++	++	+++	+++	+++	+++	+++	+++	+++	+++	++	+++
tubule interstitum, coretex		-	-	-	±	±	+	-	±	+	±	-	±	-	-	-	-
tubule interstitum, outer medulla		±	+	-	±	+	±	±	+	++	+++	++	+++	+	++	±	+++
tubule interstitum, inner medulla		±	+	-	+	+	+	-	±	+	++	±	+++	+	++	±	++
tubule interstitum, renal papilla		+	++	±	++	++	++	±	+	+++	+++	++	+++	+++	++	±	+++
Immunohistochemistry		P	P	P	P	P	P	P	P	P	P	P	P	P	P	P	P
Heart																	
Amyloidosis /Amyloid deposit																	
myocardial deposit		±	±	±	±	-	±	±	±	±	±	±	±	±	±	-	±
Immunohistochemistry		P	P	P	P	-	P	P	P	P	P	P	P	P	P	-	P
Stomach																	
Amyloidosis /Amyloid deposit																	
lamira propria		+	-	-	-	+	+	NE	NE	NE	NE	NE	NE	NE	NE	NE	NE
Immunohistochemistry		P	-	-	-	P	P	NE	NE	NE	NE	NE	NE	NE	NE	NE	NE
Duodenum																	
Amyloidosis /Amyloid deposit																	
lamira propria		±	-	-	-	+	+	NE	NE	NE	NE	NE	NE	NE	NE	NE	NE
Immunohistochemistry		P	-	-	-	P	P	NE	NE	NE	NE	NE	NE	NE	NE	NE	NE

M: male; F: female; −: no noteworthy findings; ±: minimal; +: mild; ++: moderate; +++: severe; NE: Not examined. P: Positive for anti SAA1/2 antibody in immunohistochemistry.

low-density area corresponding to amyloid deposition was observed in the glomerulus (Fig. 3C), and non-branched, nearly 10 nm-wide fibrils were observed in the mesangial area (Fig. 3D, 3E). Podocyte fusion and effacement were present in regions with the loss of primary and secondary foot processes (Fig. 3D). Overall, the fibril features observed in ultrastructural examination were consistent with those previously reported for amyloid fibrils[13].

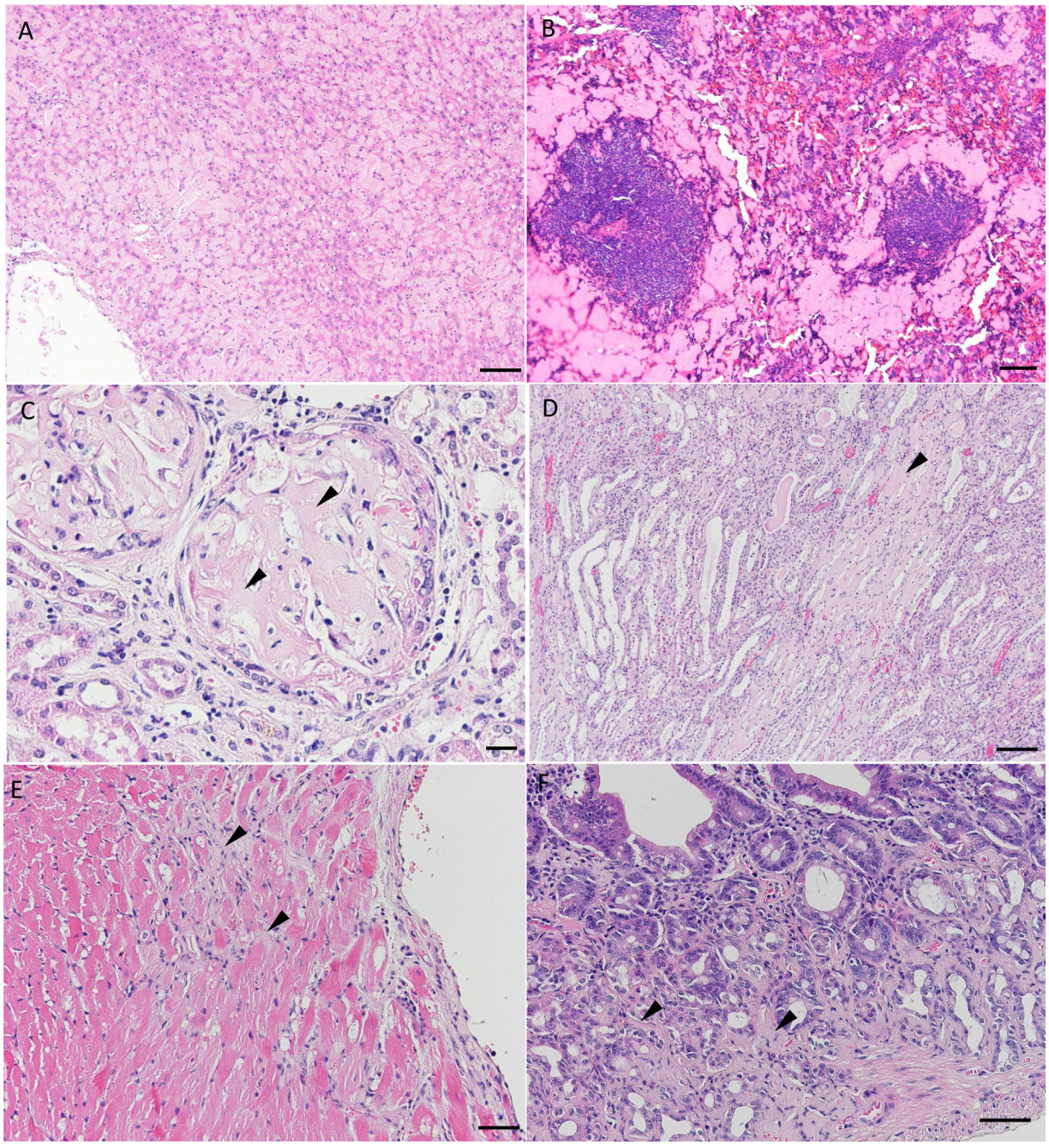

Fig. 1. Histopathology of the liver, spleen, kidney, heart, and duodenum in hematoxylin and eosin (HE)-stained specimens from CD-1 mice. A: Atrophy of hepatocytes and deposition of eosinophilic substances in the space of Disse in the liver (animal No. 7, scale bar=100 µm); B: Deposition of eosinophilic substances in the red pulp and marginal zone of the spleen (animal No. 9, scale bar=100 µm); C, D: Deposition of eosinophilic substances (arrowheads) in the glomerulus (C, scale bar=20 µm) and tubular interstitium (D, scale bar=100 µm) of the kidney (animal No. 9). Dilatation of the distal tubule and hyaline casts in the tubule were also observed; E: Atrophy of cardiomyocytes and deposition of eosinophilic substances (arrowheads) were observed in the interstitium of cardiomyocytes in the heart (animal No. 1, scale bar=50 µm); F: Deposition of eosinophilic substances (arrowheads) in the lamina propria of the duodenum (animal No. 6, scale bar=50 µm).

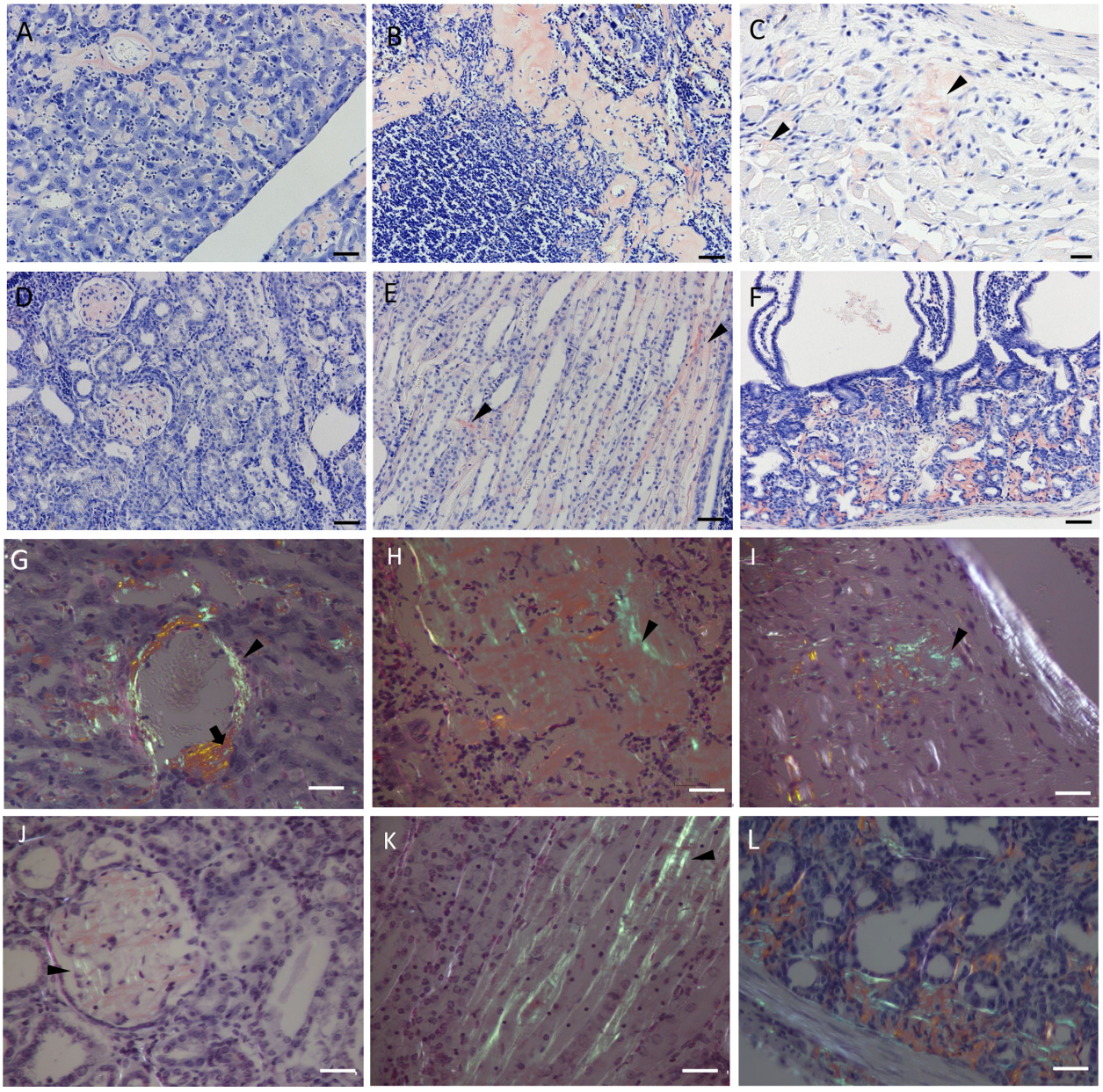

Fig. 2. Light and polarized microscopic examination of direct fast scarlet (DFS)-stained sections of the liver, spleen, heart, kidney, and duodenum from CD-1 mice. Light microscopy showed areas of DFS-positive staining in the A: perivascular area and space of Disse in the liver (animal No. 1, scale bar=50 µm); B: red pulp and marginal zone of the spleen (animal No. 9, scale bar=50 µm); C: interstitium of cardiomyocytes (arrowheads) from the heart (animal No. 1, scale bar=20 µm); D, E: glomerulus (D) and tubular interstitium (E, arrowhead) of the kidney (animal No. 14, scale bar=50 µm); and F: lamina propria of the duodenum (animal No. 6). Scale bars are 50 µm except for C, for which the scale bar is 20 µm. Under polarized conditions, areas with apple-green (arrowheads) and yellow or orange (arrow) birefringence were observed in G: perivascular area and space of Disse of the liver (animal No. 1); H: red pulp of the spleen (animal No. 9); I: interstitium of cardiomyocytes from the heart (animal No. 1); and J and K: glomerulus (J) and tubular interstitium (K) of the kidney (animal No. 14). All scale bars=20 µm.

Types of amyloidosis and precursor proteins identified in CD-1 mice

Immunohistochemistry was used to evaluate the types of amyloidosis and the amyloid precursor proteins present in CD-1 mice that had ulcerative dermatitis or inflammation in other tissues (Table 1). We hypothesized that these mice would exhibit AA amyloidosis associated with chronic inflammatory lesions. Immunohistochemical analysis showed that areas with DFS-positive staining were also positive for murine SAA1/2 antibody (Fig. 4). This result suggests that the precursor protein is SAA1/2, and that the type of amyloidosis observed in CD-1 mice is verified as AA amyloidosis.

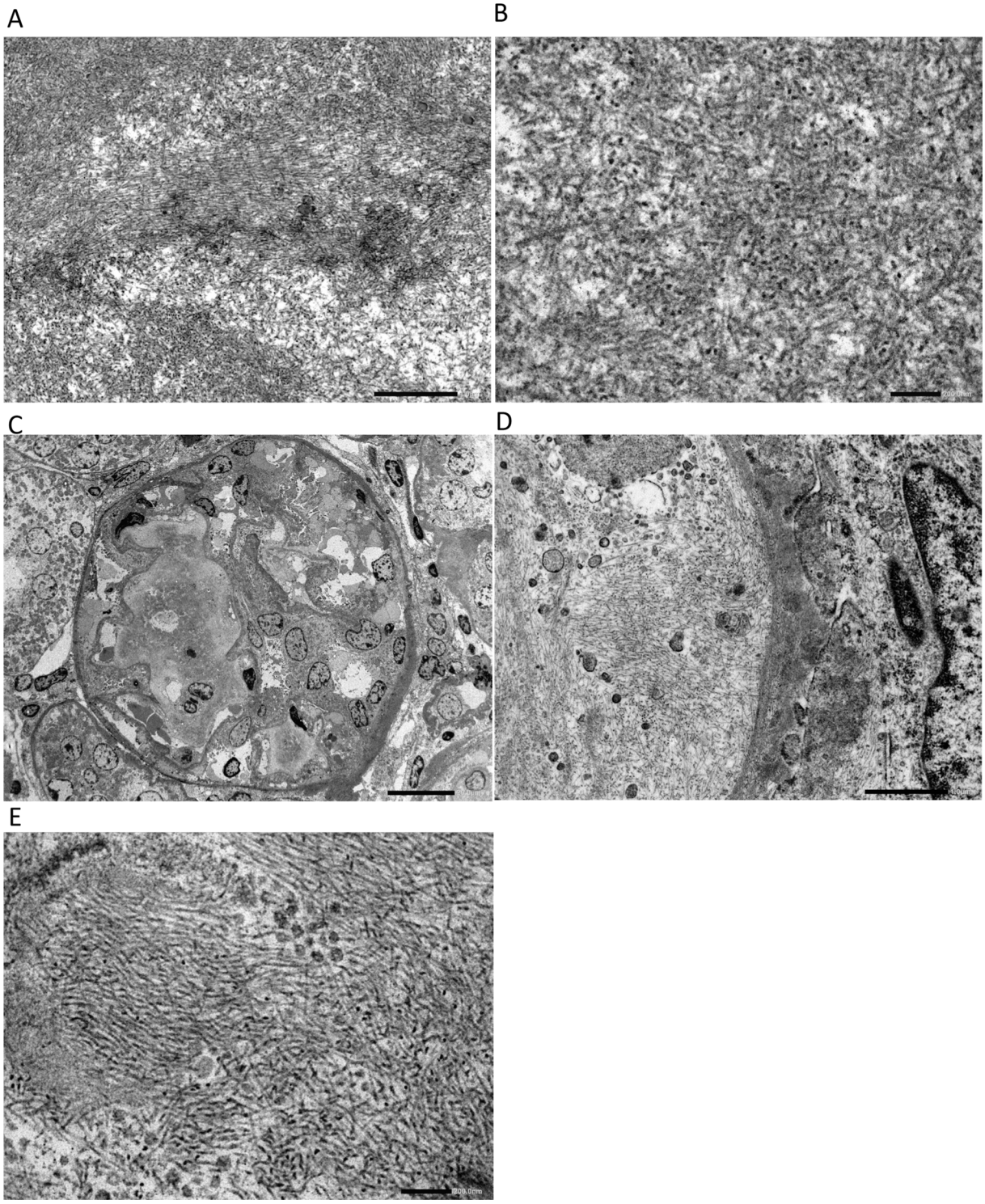

Fig. 3. Ultrastructural observation of the liver and kidney. A, B. Liver (animal No. 14). Non-branching fibril bundles were also observed. The width of the fibrils is approximately 10 nm. (Scale bar: A.=1 μm, B.=100 nm.) C, D, E. Kidney (animal No. 14). A low-density area (arrowheads) is observed in the glomeruli. Nonbranched fibrils were mainly deposited in the mesangial areas (arrows). (C) Scale bar=20 m. Fibrils were also observed in the glomerular basement membrane (GBM), with foot process fusion and effacement in podocytes (arrowheads). (D. Scale bar=1 μm.) The width of the fibrils is approximately 10 nm. (E. Scale bar=100 nm).

Amino acid sequences of amyloid deposits and common component proteins in CD-1 mice

To determine the amino acid sequence of the peptide fragments detected in the amyloid deposits in the livers of CD-1 mice, we performed LC-MS/MS analysis. The MS/MS spectra of the unique peptides for SAA1 and SAA2

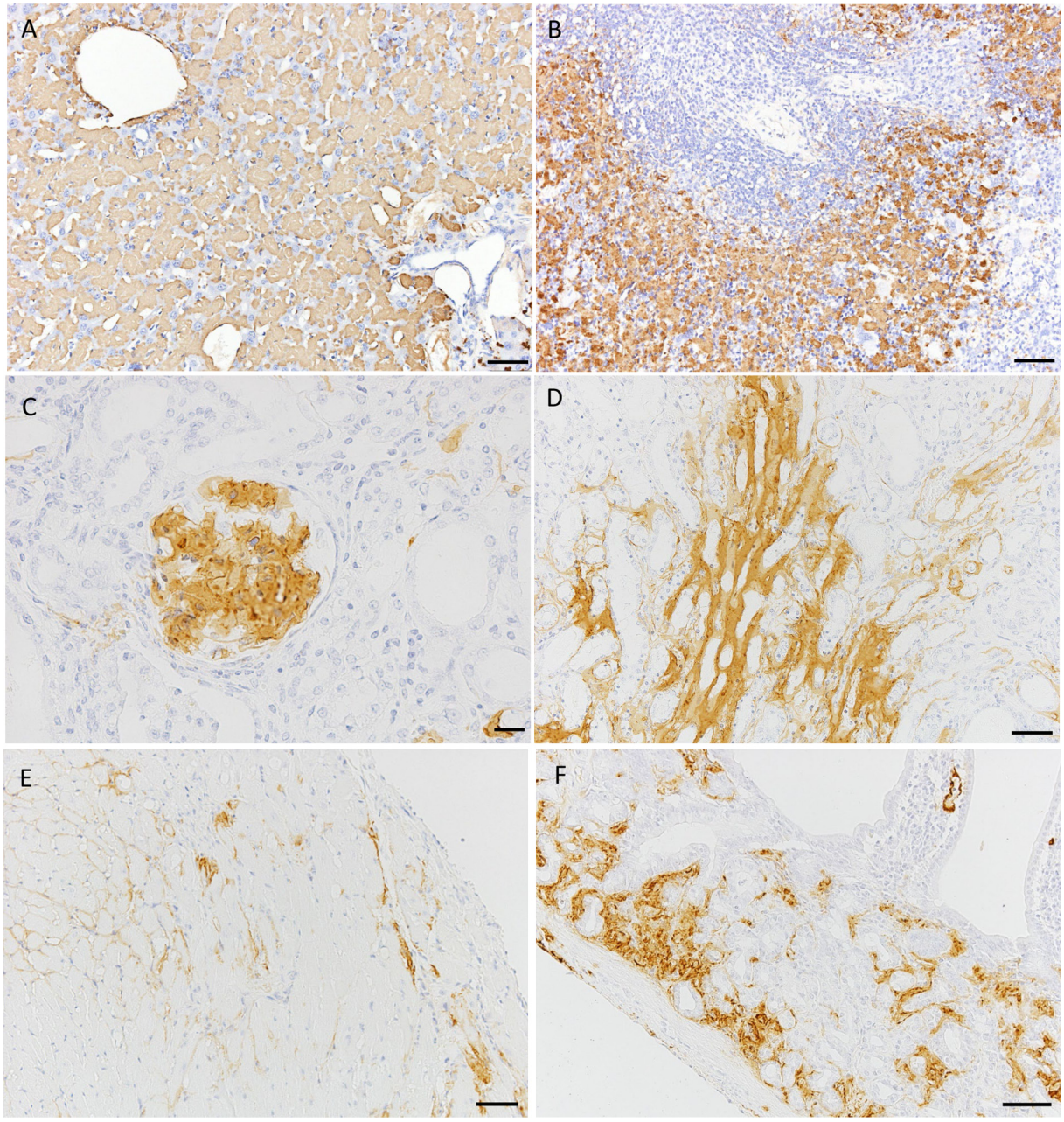

Fig. 4. Immunohistochemistry for anti-SAA1/2 antibody. Positive SAA1/2 antibody staining is observed in A: perivascular area and space of Disse of the liver (animal No. 2); B: red pulp and marginal zone of the spleen (animal No. 9); C: glomerulus and tubule interstitium from the kidney (animal No. 14); D: tubule interstitium and outer medulla of the kidney (animal No. 14); E: cardiomyocyte interstitium of the heart (animal No. 1); and F: lamina propria of the duodenum (animal No. 6). Scale bars for A, B, D, E, and F are 50 μm. The scale bar for C is 20 μm.

(Fig. 5A) and the amino acid sequences and peptide fragments detected in different mice (Fig. 5B) varied; however, the SAA1 peptide fragment 39Gly-70Arg and N-terminal SAA2 peptide fragment 6Ile-70Arg were detected in most mice that exhibited amyloidosis. The coverage of the SAA2 protein was higher than that of SAA1. To confirm the amyloid component proteins that were detectable only in CD-1 mice with amyloidosis, we selected nine animals for which the ion intensity of SAA2 was high (>1E+08), and thus, sufficient for analysis. We compared the peptides detected in these nine cases of amyloidosis in CD-1 mice with those detected in three cases of CD-1 mice without amyloidosis. In this analysis, a major protein component was determined to be associated with amyloidosis when more than two peptide fragments were detected in the nine CD-1 mice with amyloidosis. The major proteins associated with amyloidosis are listed in Fig. 6; 78 major proteins, including SAA1 and SAA2, were detected in the nine CD-1 mice with amyloi-

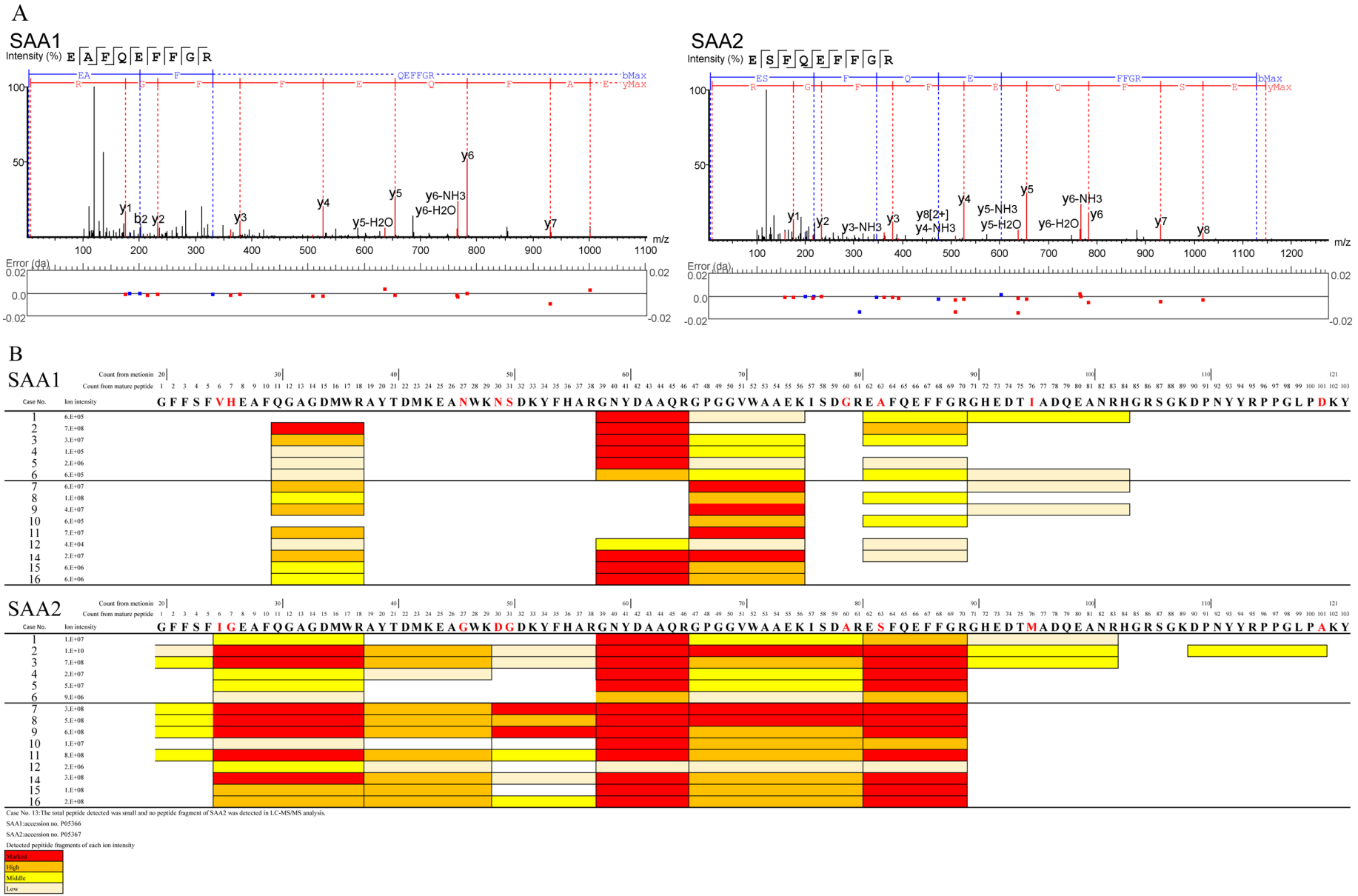

Fig. 5. LC-MS/MS analysis for amyloidosis in the liver. A. MS/MS spectrum of unique peptide fragments of SAA1 and SAA2 detected in animal No. 8. B. Amino acids sequences of SAA1 and SAA2 from the database are shown above, and the peptide fragments detected in each amyloidosis mouse are shown below. Marked, high, moderate, and low ion intensity of the peptide fragments are indicated by red, orange, yellow, and pale yellow, respectively.

dosis but were not detected in the three CD-1 mice without amyloidosis. The ion intensity of SAA2 was higher than that of SAA1 in all analyzed cases.

Copy number variations in SAA1 and SAA2 gene in mice

A CNV assay was used to confirm SAA1 and SAA2 gene copy numbers in CD-1 mice with and without amy-

			Ion intensity											
			Amyloidosis CD-1 mice									Non-amyloidosis CD-1 mice		
Accession	Description	Case No.	2	3	7	8	9	11	14	15	16	I31	I33	I38
P05367|SAA2	Serum amyloid A-2 protein _ GN=Saa2 PE=1 SV=1		1.E+10	7.E+08	3.E+08	5.E+08	6.E+08	8.E+08	3.E+08	1.E+08	2.E+08	n.d	n.d	n.d
P05366|SAA1	Serum amyloid A-1 protein _ GN=Saa1 PE=1 SV=2		7.E+08	3.E+07	6.E+07	1.E+08	4.E+07	7.E+07	2.E+07	6.E+06	6.E+06	n.d	n.d	n.d
P12246|SAMP	Serum amyloid P-component _ GN=Apcs PE=1 SV=2		3.33E+08	2.90E+08	1.66E+06	1.44E+07	3.68E+07	1.71E+06	1.63E+08	3.95E+07	3.33E+07	n.d	n.d	n.d
P29788|VTNC	Vitronectin _ GN=Vtn PE=1 SV=2		2.36E+08	1.52E+07	3.13E+07	4.78E+07	1.59E+08	1.45E+08	1.94E+07	2.91E+06	2.25E+06	n.d	n.d	n.d
P61205|ARF3	ADP-ribosylation factor 3 _ GN=Arf3 PE=2 SV=2		1.93E+08	1.19E+09	8.53E+06	1.05E+07	1.16E+07	4.56E+06	1.26E+06	1.92E+07	4.07E+08	n.d	n.d	n.d
P84078|ARF1	ADP-ribosylation factor 1 _ GN=Arf1 PE=1 SV=2		1.93E+08	1.19E+09	8.53E+06	1.05E+07	1.16E+07	4.56E+06	1.26E+06	1.92E+07	4.07E+08	n.d	n.d	n.d
Q91X72|HEMO	Hemopexin _ GN=Hpx PE=1 SV=2		1.62E+08	6.56E+07	3.00E+06	9.40E+06	2.66E+07	3.68E+07	6.13E+06	4.73E+06	4.62E+06	n.d	n.d	n.d
A6X935|ITIH4	Inter alpha-trypsin inhibitor heavy chain 4 _ GN=Itih4 PE=1 SV=2		5.96E+07	1.85E+08	2.86E+07	4.67E+07	5.16E+07	6.30E+07	5.10E+07	1.71E+07	6.69E+07	n.d	n.d	n.d
P19639|GSTM3	Glutathione S-transferase Mu 3 _ GN=Gstm3 PE=1 SV=2		5.08E+07	2.51E+07	1.86E+07	1.00E+07	1.86E+08	2.18E+07	1.30E+07	5.24E+06	3.60E+06	n.d	n.d	n.d
P01837|IGKC	Immunoglobulin kappa constant _ GN=Igkc PE=1 SV=2		4.51E+07	3.21E+07	1.26E+06	6.35E+06	3.48E+06	7.24E+06	3.11E+05	1.09E+06	1.03E+06	n.d	n.d	n.d
Q8VCM7|FIBG	Fibrinogen gamma chain _ GN=Fgg PE=1 SV=1		3.75E+07	2.74E+07	8.33E+06	5.48E+06	2.11E+07	7.52E+07	9.41E+07	6.12E+06	4.86E+06	n.d	n.d	n.d
P21981|TGM2	Protein-glutamine gamma-glutamyltransferase 2 _ GN=Tgm2 PE=1 SV=4		3.71E+07	6.67E+06	4.72E+06	9.68E+06	5.67E+07	3.95E+07	1.47E+07	1.23E+07	1.13E+07	n.d	n.d	n.d
O08709|PRDX6	Peroxiredoxin-6 _ GN=Prdx6 PE=1 SV=3		3.09E+07	1.01E+06	2.11E+06	6.18E+06	5.35E+06	3.02E+06	2.28E+06	1.08E+06	1.42E+06	n.d	n.d	n.d
P11276|FINC	Fibronectin _ GN=Fn1 PE=1 SV=4		2.92E+07	1.34E+07	2.97E+06	7.31E+05	1.80E+07	6.15E+06	4.71E+06	2.26E+06	1.47E+06	n.d	n.d	n.d
P48036|ANXA5	Annexin A5 _ GN=Anxa5 PE=1 SV=1		1.80E+07	4.33E+07	1.74E+07	1.22E+07	6.00E+07	6.11E+07	2.83E+07	1.27E+07	1.13E+07	n.d	n.d	n.d
Q61646|HPT	Haptoglobin _ GN=Hp PE=1 SV=1		1.46E+07	1.78E+06	4.45E+05	1.16E+05	2.92E+06	1.57E+06	3.11E+06	1.12E+06	7.11E+05	n.d	n.d	n.d
P11247|PERM	Myeloperoxidase _ GN=Mpo PE=1 SV=2		1.22E+07	1.41E+07	1.21E+06	9.69E+07	5.64E+06	5.19E+06	6.33E+07	1.00E+08	6.53E+07	n.d	n.d	n.d
Q9CZS1|AL1B1	Aldehyde dehydrogenase X mitochondrial _ GN=Aldh1b1 PE=1 SV=1		1.20E+07	5.68E+05	1.84E+05	2.34E+06	4.05E+07	6.42E+05	6.88E+05	2.16E+05	1.62E+05	n.d	n.d	n.d
E9PV24|FIBA	Fibrinogen alpha chain _ GN=Fga PE=1 SV=1		1.13E+07	9.38E+06	1.30E+06	1.25E+06	3.06E+07	7.21E+06	1.18E+07	6.23E+05	9.54E+05	n.d	n.d	n.d
P43277|H13	Histone H1.3 _ GN=H1-3 PE=1 SV=2		1.12E+07	3.67E+07	1.53E+06	2.87E+06	1.39E+07	1.22E+07	3.46E+06	1.15E+06	9.26E+05	n.d	n.d	n.d
Q8K0E8|FIBB	Fibrinogen beta chain _ GN=Fgb PE=1 SV=1		1.04E+07	6.43E+06	6.32E+05	1.15E+06	2.65E+06	1.45E+06	1.65E+07	7.22E+06	6.08E+06	n.d	n.d	n.d
O09173|HGD	Homogentisate 1 2-dioxygenase _ GN=Hgd PE=1 SV=2		1.03E+07	3.40E+06	4.43E+06	4.14E+06	1.15E+07	7.42E+06	6.34E+06	2.73E+06	3.46E+06	n.d	n.d	n.d
P47738|ALDH2	Aldehyde dehydrogenase mitochondrial _ GN=Aldh2 PE=1 SV=1		9.77E+06	5.40E+07	3.17E+06	1.24E+06	1.17E+07	8.89E+05	5.56E+06	1.78E+06	2.02E+06	n.d	n.d	n.d
P01027|CO3	Complement C3 _ GN=C3 PE=1 SV=3		8.85E+06	2.17E+06	1.79E+06	1.06E+06	1.53E+07	2.94E+06	7.30E+06	1.74E+06	8.92E+05	n.d	n.d	n.d
Q9QXS1|PLEC	Plectin _ GN=Plec PE=1 SV=3		7.07E+06	3.04E+06	3.08E+06	2.38E+06	3.30E+06	2.35E+06	5.49E+06	1.93E+06	1.16E+06	n.d	n.d	n.d
Q8R0W0|EPIPL	Epiplakin _ GN=Eppk1 PE=1 SV=2		6.28E+06	2.89E+06	7.41E+06	6.82E+06	1.50E+07	1.62E+07	1.63E+07	5.87E+05	3.25E+06	n.d	n.d	n.d
P62849|RS24	Small ribosomal subunit protein eS24 _ GN=Rps24 PE=1 SV=1		5.61E+06	1.37E+07	9.55E+05	8.18E+05	1.23E+07	1.83E+06	2.65E+06	1.11E+06	9.94E+05	n.d	n.d	n.d
Q06890|CLUS	Clusterin _ GN=Clu PE=1 SV=1		5.26E+06	6.18E+06	1.46E+06	3.92E+06	1.87E+07	2.65E+06	2.09E+06	7.47E+05	2.48E+05	n.d	n.d	n.d
P25444|RS2	Small ribosomal subunit protein uS5 _ GN=Rps2 PE=1 SV=3		4.95E+06	1.97E+07	3.89E+06	6.14E+05	3.22E+07	2.84E+06	6.98E+06	2.49E+06	1.76E+06	n.d	n.d	n.d
Q91ZX7|LRP1	Prolow-density lipoprotein receptor-related protein 1 _ GN=Lrp1 PE=1 SV=1		4.88E+06	2.85E+06	6.66E+05	7.36E+05	3.50E+06	4.59E+05	1.32E+06	9.52E+05	7.74E+05	n.d	n.d	n.d
P62984|RL40	Ubiquitin-ribosomal protein eL40 fusion protein _ GN=Uba52 PE=1 SV=2		4.74E+06	1.69E+07	1.52E+06	3.88E+06	9.36E+06	8.47E+05	3.98E+06	2.27E+06	1.82E+06	n.d	n.d	n.d
P0DP27|CALM2	Calmodulin-2 _ GN=Calm2 PE=1 SV=1		4.49E+06	2.42E+06	4.35E+05	6.68E+05	1.61E+06	1.13E+06	2.81E+06	1.11E+06	7.53E+05	n.d	n.d	n.d
P0DP26|CALM1	Calmodulin-1 _ GN=Calm1 PE=1 SV=1		4.49E+06	2.42E+06	4.35E+05	6.68E+05	1.61E+06	1.13E+06	2.81E+06	1.11E+06	7.53E+05	n.d	n.d	n.d
P0DP28|CALM3	Calmodulin-3 _ GN=Calm3 PE=1 SV=1		4.49E+06	2.42E+06	4.35E+05	6.68E+05	1.61E+06	1.13E+06	2.81E+06	1.11E+06	7.53E+05	n.d	n.d	n.d
P07724|ALBU	Albumin _ GN=Alb PE=1 SV=3		4.38E+06	2.80E+06	4.37E+06	7.95E+05	9.63E+06	1.04E+07	2.94E+06	1.96E+06	2.39E+06	n.d	n.d	n.d
Q9D1R9|RL34	Large ribosomal subunit protein eL34 _ GN=Rpl34 PE=1 SV=2		4.11E+06	5.77E+05	3.73E+05	6.56E+05	1.12E+07	1.33E+05	7.64E+05	8.95E+05	6.34E+05	n.d	n.d	n.d
P49429|HPPD	4-hydroxyphenylpyruvate dioxygenase _ GN=Hpd PE=1 SV=3		4.06E+06	1.32E+06	1.60E+06	5.55E+06	1.16E+07	7.27E+05	3.78E+06	9.60E+05	1.55E+06	n.d	n.d	n.d
P18760|COF1	Cofilin-1 _ GN=Cfl1 PE=1 SV=3		3.99E+06	2.46E+07	1.29E+06	2.10E+06	8.98E+06	2.33E+06	2.49E+06	1.58E+06	1.54E+06	n.d	n.d	n.d
Q60605|MYL6	Myosin light polypeptide 6 _ GN=Myl6 PE=1 SV=3		3.65E+06	5.57E+06	2.44E+05	6.31E+05	1.84E+06	2.52E+05	4.97E+05	7.79E+05	1.80E+06	n.d	n.d	n.d
Q9CRB3|HIUH	5-hydroxyisourate hydrolase _ GN=Urah PE=1 SV=1		3.37E+06	8.12E+06	1.79E+06	9.97E+05	2.05E+07	3.41E+06	3.82E+06	1.45E+06	1.01E+06	n.d	n.d	n.d
P35979|RL12	Large ribosomal subunit protein uL11 _ GN=Rpl12 PE=1 SV=2		3.33E+06	1.28E+06	9.02E+05	5.57E+05	1.94E+07	4.09E+05	2.96E+05	1.51E+06	1.25E+06	n.d	n.d	n.d
Q922R8|PDIA6	Protein disulfide-isomerase A6 _ GN=Pdia6 PE=1 SV=3		3.29E+06	2.92E+07	1.96E+06	5.30E+06	2.56E+07	3.11E+06	1.88E+07	3.18E+06	2.40E+06	n.d	n.d	n.d
P24456|CP2DA	Cytochrome P450 2D10 _ GN=Cyp2d10 PE=1 SV=2		3.25E+06	1.90E+06	1.06E+06	9.88E+05	7.29E+06	2.49E+06	3.42E+06	8.59E+05	1.68E+06	n.d	n.d	n.d
P27773|PDIA3	Protein disulfide-isomerase A3 _ GN=Pdia3 PE=1 SV=2		3.21E+06	6.49E+06	4.48E+05	1.88E+05	9.26E+06	1.89E+06	5.63E+06	1.12E+06	1.25E+06	n.d	n.d	n.d
P14824|ANXA6	Annexin A6 _ GN=Anxa6 PE=1 SV=3		2.37E+06	1.83E+06	5.39E+06	1.60E+06	7.28E+06	2.00E+07	7.00E+06	1.78E+06	2.79E+06	n.d	n.d	n.d
Q8BT60|CPNE3	Copine-3 _ GN=Cpne3 PE=1 SV=2		2.08E+06	2.45E+07	2.39E+06	1.51E+05	2.71E+06	3.61E+06	2.38E+06	8.00E+05	1.25E+07	n.d	n.d	n.d
P01029|CO4B	Complement C4-B _ GN=C4b PE=1 SV=3		2.03E+06	5.80E+05	1.01E+06	8.46E+05	2.16E+06	1.36E+06	3.03E+06	3.49E+05	1.73E+05	n.d	n.d	n.d
P55264|ADK	Adenosine kinase _ GN=Adk PE=1 SV=2		1.98E+06	1.04E+07	2.86E+05	3.58E+06	2.43E+07	1.83E+05	1.80E+06	1.85E+06	1.51E+06	n.d	n.d	n.d
P63242|IF5A1	Eukaryotic translation initiation factor 5A-1 _ GN=Eif5a PE=1 SV=2		1.96E+06	1.84E+06	1.47E+06	7.48E+05	1.08E+07	1.87E+06	9.21E+06	2.83E+06	2.50E+06	n.d	n.d	n.d
P01633|KV5A1	Immunoglobulin kappa chain variable 6-17 _ GN=Igkv6-17 PE=1 SV=1		1.90E+06	1.02E+06	3.28E+05	1.20E+05	7.88E+05	2.78E+06	4.31E+05	2.04E+05	1.82E+05	n.d	n.d	n.d
P00405|COX2	Cytochrome c oxidase subunit 2 _ GN=Mtco2 PE=1 SV=1		1.73E+06	1.09E+07	4.96E+05	9.43E+05	6.81E+06	1.33E+05	9.03E+05	4.27E+05	5.33E+05	n.d	n.d	n.d
Q99K67|AASS	Alpha-aminoadipic semialdehyde synthase mitochondrial _ GN=Aass PE=1 SV=1		1.65E+06	2.52E+07	1.17E+06	1.45E+05	1.49E+06	6.93E+05	1.14E+06	3.18E+05	2.42E+05	n.d	n.d	n.d
Q9DBT9|M2GD	Dimethylglycine dehydrogenase mitochondrial _ GN=Dmgdh PE=1 SV=1		1.64E+06	7.64E+06	4.74E+06	3.98E+05	5.48E+06	1.29E+06	8.42E+06	2.05E+06	1.66E+06	n.d	n.d	n.d
Q61147|CERU	Ceruloplasmin _ GN=Cp PE=1 SV=2		1.57E+06	1.28E+06	1.04E+06	2.63E+05	1.18E+06	7.23E+05	1.48E+06	6.39E+05	4.34E+05	n.d	n.d	n.d
Q3THE2|ML12B	Myosin regulatory light chain 12B _ GN=Myl12b PE=1 SV=2		1.55E+06	1.75E+06	1.69E+06	1.69E+06	7.86E+06	1.04E+06	4.11E+06	2.33E+06	1.90E+06	n.d	n.d	n.d
P58771|TPM1	Tropomyosin alpha-1 chain _ GN=Tpm1 PE=1 SV=1		1.50E+06	7.49E+06	1.17E+06	1.14E+06	3.73E+06	3.79E+07	8.06E+07	1.01E+08	6.43E+07	n.d	n.d	n.d
P53026|RL10A	Large ribosomal subunit protein uL1 _ GN=Rpl10a PE=1 SV=3		1.36E+06	1.17E+07	4.91E+06	2.37E+06	3.75E+06	6.85E+05	2.77E+06	1.12E+06	7.25E+05	n.d	n.d	n.d
Q9D3D9|ATPD	ATP synthase subunit delta mitochondrial _ GN=Atp5f1d PE=1 SV=1		1.35E+06	1.61E+06	3.90E+06	2.17E+05	2.69E+06	1.00E+06	1.21E+06	1.44E+06	1.33E+06	n.d	n.d	n.d
Q99PL5|RRBP1	Ribosome-binding protein 1 _ GN=Rrbp1 PE=1 SV=2		1.21E+06	8.27E+06	3.66E+05	2.36E+05	1.22E+07	2.57E+05	1.00E+06	1.05E+06	7.16E+05	n.d	n.d	n.d
P25688|URIC	Uricase _ GN=Uox PE=1 SV=2		1.16E+06	1.12E+06	1.61E+06	1.11E+05	3.25E+06	1.09E+06	3.71E+06	1.92E+06	1.40E+06	n.d	n.d	n.d
P01631|KV2A7	Ig kappa chain V-II region 26-10 _ PE=1 SV=1		1.08E+06	1.02E+06	4.59E+05	1.73E+06	4.09E+06	3.02E+06	1.80E+05	2.77E+05	2.18E+05	n.d	n.d	n.d
P62751|RL23A	Large ribosomal subunit protein uL23 _ GN=Rpl23a PE=1 SV=1		1.02E+06	2.38E+05	9.78E+05	1.22E+06	3.12E+06	7.29E+05	4.40E+05	3.95E+05	3.26E+05	n.d	n.d	n.d
Q05793|PGBM	Basement membrane-specific heparan sulfate proteoglycan core protein _ GN=Hspg2 PE=1 SV=1		9.70E+05	6.95E+05	1.07E+06	1.09E+06	4.19E+06	3.82E+05	2.18E+05	2.85E+05	1.72E+05	n.d	n.d	n.d
P57780|ACTN4	Alpha-actinin-4 _ GN=Actn4 PE=1 SV=1		9.58E+05	5.35E+05	2.62E+05	1.01E+05	7.24E+06	2.79E+05	1.20E+06	6.59E+05	4.75E+05	n.d	n.d	n.d
Q61838|PZP	Pregnancy zone protein _ GN=Pzp PE=1 SV=3		8.22E+05	2.18E+06	1.54E+06	2.70E+05	2.50E+06	1.33E+06	1.87E+06	2.04E+06	1.48E+06	n.d	n.d	n.d
P14602|HSPB1	Heat shock protein beta-1 _ GN=Hspb1 PE=1 SV=3		7.79E+05	2.73E+05	1.50E+06	1.95E+05	1.36E+06	2.66E+05	1.15E+06	1.64E+06	1.05E+06	n.d	n.d	n.d
P63163|RSMN	Small nuclear ribonucleoprotein-associated protein N _ GN=Snrpn PE=1 SV=1		7.30E+05	1.43E+05	1.28E+06	2.70E+05	6.01E+05	1.21E+06	1.96E+06	5.84E+05	4.37E+05	n.d	n.d	n.d
P27048|RSMB	Small nuclear ribonucleoprotein-associated protein B _ GN=Snrpb PE=1 SV=1		7.30E+05	1.43E+05	1.28E+06	2.70E+05	6.01E+05	1.21E+06	1.96E+06	5.84E+05	4.37E+05	n.d	n.d	n.d
Q02257|PLAK	Junction plakoglobin _ GN=Jup PE=1 SV=3		6.01E+05	6.49E+05	2.65E+06	5.40E+05	2.32E+06	8.50E+05	1.76E+05	3.74E+06	2.76E+06	n.d	n.d	n.d
P40142|TKT	Transketolase _ GN=Tkt PE=1 SV=1		5.98E+05	5.48E+06	1.52E+06	7.37E+05	2.22E+06	4.40E+05	1.37E+06	8.24E+05	6.89E+05	n.d	n.d	n.d
P07356|ANXA2	Annexin A2 _ GN=Anxa2 PE=1 SV=2		5.68E+05	5.48E+06	1.03E+06	7.10E+05	1.54E+06	1.19E+06	2.06E+06	1.31E+06	1.41E+06	n.d	n.d	n.d
P07901|HS90A	Heat shock protein HSP 90-alpha _ GN=Hsp90aa1 PE=1 SV=4		3.70E+05	6.93E+05	5.94E+05	1.02E+05	8.40E+05	4.15E+05	2.04E+06	1.01E+06	3.40E+05	n.d	n.d	n.d
P50172|DHI1	11-beta-hydroxysteroid dehydrogenase 1 _ GN=Hsd11b1 PE=1 SV=3		3.14E+05	5.01E+05	7.70E+05	2.01E+06	4.96E+06	6.39E+05	1.43E+06	1.52E+05	1.36E+05	n.d	n.d	n.d
Q91X52|DCXR	L-xylulose reductase _ GN=Dcxr PE=1 SV=2		2.72E+05	2.79E+06	1.33E+06	3.37E+05	8.51E+06	1.13E+06	1.59E+06	2.39E+05	8.49E+05	n.d	n.d	n.d
Q8CC86|PNCB	Nicotinate phosphoribosyltransferase _ GN=Naprt PE=1 SV=1		2.49E+05	7.32E+05	2.67E+05	1.37E+05	2.07E+06	1.69E+05	5.56E+05	2.08E+05	2.16E+05	n.d	n.d	n.d
P26039|TLN1	Talin-1 _ GN=Tln1 PE=1 SV=2		2.42E+05	3.81E+06	8.55E+05	1.57E+06	8.58E+06	7.12E+05	8.29E+05	5.52E+05	4.60E+05	n.d	n.d	n.d
P52196|THTR	Thiosulfate sulfurtransferase _ GN=Tst PE=1 SV=3		1.53E+05	1.20E+05	6.78E+05	1.98E+05	7.99E+05	1.32E+05	4.29E+05	5.31E+05	6.24E+05	n.d	n.d	n.d
P20108|PRDX3	Thioredoxin-dependent peroxide reductase mitochondrial _ GN=Prdx3 PE=1 SV=1		1.26E+05	2.40E+06	1.27E+06	1.22E+05	1.55E+06	3.56E+06	2.88E+06	9.81E+05	3.85E+05	n.d	n.d	n.d

OS: Mus musculus; OX: 10090. n.d: not detected. Each ion intensity of protein is shown in color scale.

Fig. 6. Proteins that were detected in nine CD-1 mice with amyloidosis but not in three CD-1 mice without amyloidosis.

loidosis, as well as in other mouse species. The copy numbers of SAA1 and SAA2 gene in each group are shown in Fig. 7A and 7B, and the results for individual cases are listed in Supplementary Table 1.

The copy numbers of SAA1 and SAA2 for each case are shown in Fig. 7C. Copy number variations of SAA1 and SAA2 were observed in both CD-1 mice with and without amyloidosis; however, the copy number tended to be higher in amyloidosis CD-1 mice than that in non-amyloidosis CD-1 mice (copy number in non-amyloidosis CD-1 mice: approx. 1–4 and 1–5 in SAA1 and SAA2 gene, respectively; amyloidosis CD-1 mice: approx. 3–4 and 4–5 in *SAA1* and *SAA2* gene, respectively). In contrast, the C3H/He mice had low copy numbers of SAA1 and SAA2 genes.

Discussion

In this study, we identified the types and precursor proteins of amyloidosis in CD-1 mice, which are used for toxicity studies. The results indicated that the type of systemic amyloidosis in CD-1 mice is AA amyloidosis, which is known to occur secondary to inflammation, and its precursor protein is SAA.

Amyloidosis is known age-related disease in mice. In CD-1 mice, the incidence of amyloidosis remains low until 52 weeks of age. When mice are older than 80 weeks of age, amyloidosis is the main cause of death and mortality in in toxicity studies[8]. In the present study, CD-1 mice with amyloidosis ranged between 47 and 104 weeks of age, and the endpoint was either moribund sacrifice or death (Table 1). These animals showed severe amyloid deposition in the liver, spleen, and kidneys (Table 2), which is consistent with previous reports for CD-1 mice with amyloidosis[8, 9]. Ultrastructural examination revealed that the deposits comprised fibrils with features consistent with amyloid formation[13].

Immunohistochemistry and LC-MS/MS revealed that CD-1 mice had AA amyloidosis, a systemic form of the disease derived from the precursor protein SAA[1]. In humans and animals, AA amyloidosis is associated with inflammation[14, 15]. Increased amounts of circulating SAA under

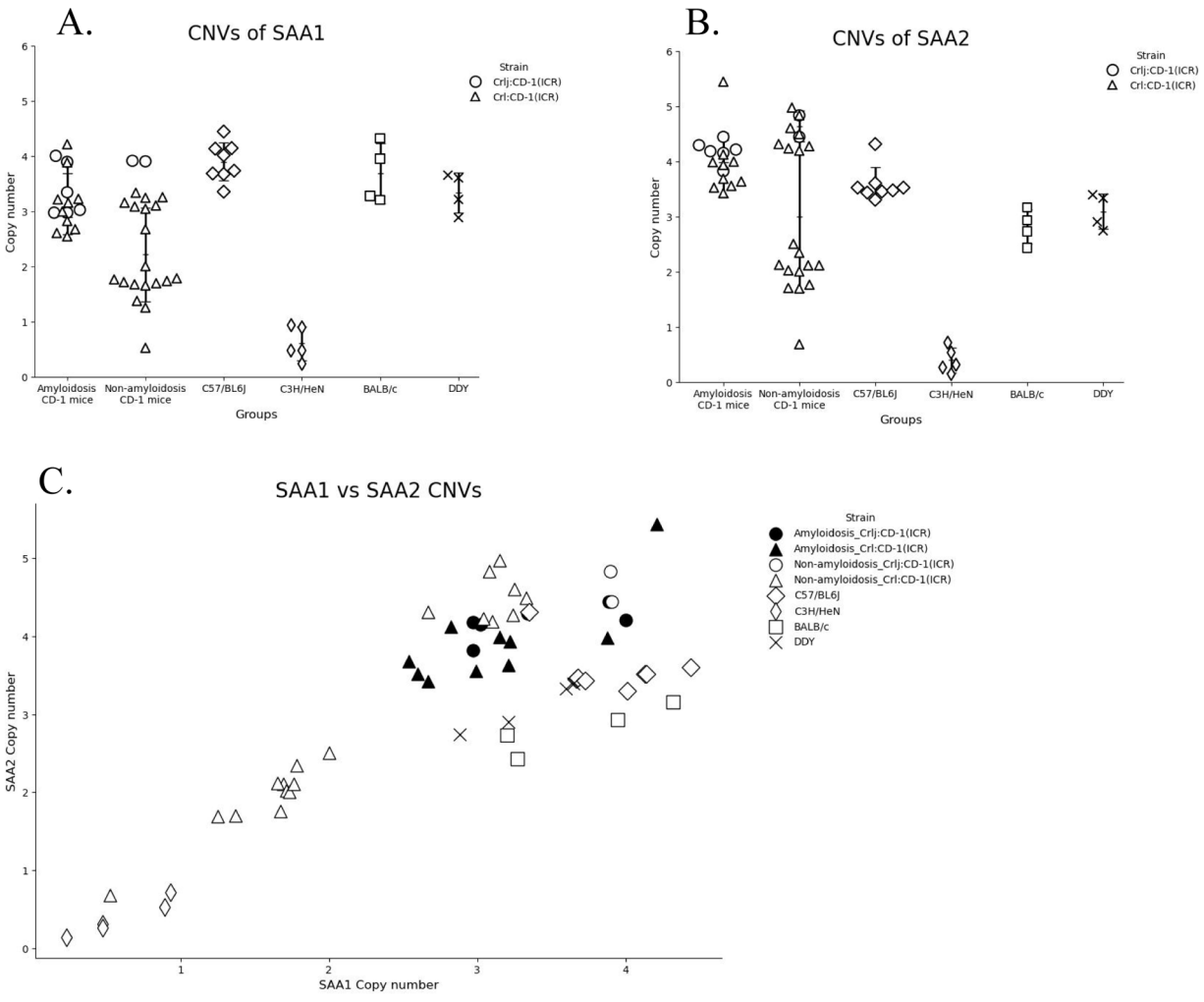

Fig. 7. Copy number variation assay. The copy number for A: SAA1 and B: SAA2 gene in each group was determined. C: *SAA1* and *SAA2* copy numbers for individual animals. Colored markers indicated animals with amyloidosis.

chronic inflammatory conditions induce the formation and aggregation of AA fibrils[16, 17]. In the present study, some mice with amyloidosis had inflammatory lesions, such as dermatitis ulcerations (Table 1).

In toxicity studies involving CD-1 mice, a high incidence of amyloidosis and skin lesions occurs owing to scratching or fighting[9, 17, 18]. Therefore, in CD-1 mice, inflammatory lesions appear to induce an increase in SAA levels and AA amyloid formation. The SAA gene family in mice consists of four members (*SAA1* to *SAA4*) that are expressed by genes on chromosome 7. The amino acid sequences of SAA1 and SAA2 are highly homologous, and only nine amino acid residues differ in the 103-residue peptide. SAA1 and 2 are known as acute-phase proteins under inflammatory conditions, and are expressed in equal amounts[19]. The LC-MS/MS analysis identified unique SAA1 and SAA2 peptide fragments (Accession No. P05366 and P05367, respectively), which were detected in the livers of the CD-1 mice with amyloidosis. The results of proteomic analyses were consistent with those of immunohistochemistry, suggesting that amyloid deposition in organs and tissues of CD-1 mice originated from SAA1 or SAA2. The amino acid sequence of SAA2 is more amyloidogenic than that of SAA1 in mice[20] and a previous study on experimental AA amyloidosis in a mouse model detected only SAA2[21]. Cryo-electron microscopy analysis of AA amyloid fibrils extracted from mice with AA amyloidosis revealed that the N-terminal region of SAA2 (Gly1-Gly69) contains nine β strands (β1–9), whereas the C-terminal region (Arg70–Tyr103) was not part of the amyloid fibril[21]. Our MS/MS analysis of CD-1 mice with amyloidosis detected SAA2 peptide fragments (Fig. 5B) that contained eight β strands (including residues that are part of β2 to β9) from the NH2-terminal. Moreover, we found that the coverage and SAA2 scores were higher than those of SAA1 in CD-1 mice with amyloidosis (Fig. 5B and Fig. 6). These results suggest that the amyloid fibrils in the mice in this study primarily comprise SAA2 and that SAA1 is incorporated into amyloid fibrils formed from SAA2. In future studies, mass spectrometry imaging could be used to detect unique SAA1 peptide fragments in these amyloid deposits.

In AA amyloidosis, some proteins have been reported to be common constituents of amyloid deposition in both humans[22] and in animals[23, 24]. Mass spectrometry imaging analysis of AA amyloidosis in the human liver showed co-deposition of vitronectin, serum amyloid P, and apolipoprotein E[22]. In the present study, vitronectin and serum amyloid P were detected only in the tissues of nine CD-1 mice with amyloidosis (Fig. 6), whereas apolipoprotein E was detected in both the presence and absence of amyloidosis (Supplementary Table 2). This result suggests that the pretreatment method[12] using DMSO could elute the common constituent proteins of AA amyloidosis. Although ApoA2 amyloidosis has been reported in mice[5], ApoA2 peptide fragments were not detected in CD-1 mice with amyloidosis. A lower incidence of ApoA2 amyloidosis has been reported in CD-1 mice based on ApoA2 amino acid sequences[3], which would support our proteomic analysis results.

In the present study, we hypothesized that CNVs are associated with AA amyloidosis. Genomic CNVs such as deletions, duplications, or other rearrangements can lead to the loss or gain of genetic material[10]. Several diseases associated with CNVs have been reported to occur[11]; therefore, we hypothesized that CNVs are the cause of the higher frequency of AA amyloidosis in CD-1 mice than in other mouse species. In our CNV assay, we found CNVs in the SAA1 and SAA2 gene of CD-1 mice without AA amyloidosis. No differences were observed in the CNVs of CD-1 mice between pre- (Crlj) and post- (Crl) Institute for Genomic Standardizations (IGS). The CNVs observed in the CD-1 mice could be attributed to their genetic background, as they are an outbred species maintained in a closed colony.

Furthermore, the copy numbers of SAA1 and SAA2 genes tended to be high, suggesting that SAA1 and SAA2 are duplicated in CD-1 mice with amyloidosis (Fig. 7). In humans, the copy numbers of SAA1 and SAA2 genes have been reported to be correlated with the baseline levels of SAA1 and SAA2 protein in the serum[25]. Similarly, in CD-1 mice, higher genomic copy numbers of SAA1 and SAA2 may lead to higher transcription and translation levels of SAA1 and SAA2 proteins in the serum. The high concentration of SAA expression in the presence of chronic inflammatory conditions may contribute to the formation of AA amyloid fibrils and subsequent development of AA amyloidosis[16]. The high genomic copy numbers of SAA1 and SAA2 may contribute to an increase in SAA1 and SAA2 expression and the formation of amyloid fibrils under chronic inflammatory conditions in CD-1 mice; however, we were unable to measure the levels of SAA1 and SAA2 in the serum in the presence or absence of inflammatory conditions such as skin ulceration.

We also compared the genomic copy numbers of SAA1 and SAA2 in different mouse species. The incidence of amyloidosis in carcinogenicity studies differs between CD-1 and B6C3F1 mice, which have high and low incidence of amyloidosis, respectively[9]. We determined the CNVs in C57/BL6 and C3H/He mice, which are the parent strains of B6C3F1 mice. C3H/He mice had lower genomic copy numbers of SAA1 and SAA2 than CD-1 mice with amyloidosis. There are many reports on the incidence of spontaneous non-neoplastic lesions such as amyloidosis in aged CD-1 and B6C3F1 mice[8, 9, 26–28] used in toxicological studies. However, we were unable to find information regarding the incidence of spontaneous systemic amyloidosis in C3H/He and C57/BL6 mice in long-term toxicity studies, likely because these mice are used less frequently than other mouse species (e.g., CD-1 or B6C3F1 mice).

Background information for some strains indicates that spontaneous amyloidosis is less common in C3H/He mice[29, 30], whereas some reports have shown spontaneous age-related amyloidosis in C57/BL6 mice[31, 32]. However, these studies only identified ApoA2 amyloidosis in C57/BL6 mice, in which the SAA protein was not detected by immunohistochemistry[5]. The low copy number of SAA gene in

C3H/He mice may have contributed to the low incidence of AA amyloidosis in B6C3F1 mice, although the incidence of AA amyloidosis in B6C3F1 mice is unclear. Moreover, the lower incidence of inflammatory lesions in B6C3F1 mice than in CD-1 mice[26, 27] may be an alternative explanation for the difference in the incidence of AA amyloidosis between different mouse species.

In conclusion, we determined the type of amyloidosis that occurs in CD-1 mice used in toxicity studies. Our results indicate that the spontaneous amyloidosis observed in toxicological studies and previously reported in CD-1 mice is AA amyloidosis. To the best of our knowledge, this is the first report describing the types of spontaneous amyloidosis observed in mice used in toxicological studies.

Additionally, we determined CNVs in SAA1 and SAA2 genes in CD-1 mice, which were higher in mice with AA amyloidosis than in C3H/He mice. This result suggests that increased CNVs might contribute to the high incidence of AA amyloidosis in CD-1 mice and the low incidence of amyloidosis in B6C3F1 mice, although other factors, such as differences in the frequency of inflammation, may also play a role. To further understand the association between AA amyloidosis and CNVs, it is important to confirm that the CD-1 mice with high copy numbers of SAA1 and 2 also have higher serum levels of SAA1 and SAA2, especially under chronic inflammatory conditions. Assessing CNVs of SAA gene in humans and animals may contribute to a better understanding of the pathogenesis of AA amyloidosis.

Disclosure of Potential Conflicts of Interest: The authors declare that there are no conflicts of interest.

Acknowledgments: The authors are grateful to Dr. Yuko Yamaguchi and the BoZo Research Center, Inc., for providing the FFPE of CD-1 mice with amyloidosis for this study. The authors are also grateful to Dr. Satomi Nishikawa, the members of the safety research laboratories at Mitsubishi Tanabe Pharma Corporation, and the members of the veterinary pathology laboratory at Azabu University.

References

1. Buxbaum JN, Dispenzieri A, Eisenberg DS, Fändrich M, Merlini G, Saraiva MJM, Sekijima Y, and Westermark P. Amyloid nomenclature 2022: update, novel proteins, and recommendations by the International Society of Amyloidosis (ISA) Nomenclature Committee. Amyloid. **29**: 213–219. 2022. [Medline] [CrossRef]
2. Merlini G, and Bellotti V. Molecular mechanisms of amyloidosis. N Engl J Med. **349**: 583–596. 2003. [Medline] [CrossRef]
3. Higuchi K, Kitagawa K, Naiki H, Hanada K, Hosokawa M, and Takeda T. Polymorphism of apolipoprotein A-II (apoA-II) among inbred strains of mice. Relationship between the molecular type of apoA-II and mouse senile amyloidosis. Biochem J. **279**: 427–433, 427–433. 1991. [Medline] [CrossRef]
4. Higuchi K, Yonezu T, Kogishi K, Matsumura A, Takeshita S, Higuchi K, Kohno A, Matsushita M, Hosokawa M, and Takeda T. Purification and characterization of a senile amyloid-related antigenic substance (apoSASSAM) from mouse serum. apoSASSAM is an apoA-II apolipoprotein of mouse high density lipoproteins. J Biol Chem. **261**: 12834–12840. 1986. [Medline] [CrossRef]
5. Li Y, Dai J, Kametani F, Yazaki M, Ishigami A, Mori M, Miyahara H, and Higuchi K. Renal function in aged C57BL/6J mice is impaired by deposition of age-related apolipoprotein A-II amyloid independent of kidney aging. Am J Pathol. **193**: 725–739. 2023. [Medline] [CrossRef]
6. Iwaide S, Oba R, Kobayashi N, and Murakami T. Local administration of amyloid enhancing factor initiates in situ amyloid A deposition followed by systemic lesions in mice. Exp Anim. **72**: 218–223. 2023. [Medline] [CrossRef]
7. McAdam KP, and Sipe JD. Murine model for human secondary amyloidosis: genetic variability of the acute-phase serum protein SAA response to endotoxins and casein. J Exp Med. **144**: 1121–1127. 1976. [Medline] [CrossRef]
8. Frith CH, and Chandra M. Incidence, distribution, and morphology of amyloidosis in Charles Rivers CD-1 mice. Toxicol Pathol. **19**: 123–127. 1991. [Medline] [CrossRef]
9. Majeed SK. Survey on spontaneous systemic amyloidosis in aging mice. Arzneimittelforschung. **43**: 170–178. 1993. [Medline]
10. Shaikh TH. Copy number variation disorders. Curr Genet Med Rep. **5**: 183–190. 2017. [Medline] [CrossRef]
11. McNaughton D, Knight W, Guerreiro R, Ryan N, Lowe J, Poulter M, Nicholl DJ, Hardy J, Revesz T, Lowe J, Rossor M, Collinge J, and Mead S. Duplication of amyloid precursor protein (APP), but not prion protein (PRNP) gene is a significant cause of early onset dementia in a large UK series. Neurobiol Aging. **33**: 426.e13–426.e21. 2012. [Medline] [CrossRef]
12. Kamiie J, Aihara N, Uchida Y, Kobayashi D, Yoshida Y, Kuroda T, Sakaue M, Sugihara Y, Rezeli M, and Marko-Varga G. Amyloid-specific extraction using organic solvents. MethodsX. **7**: 100770. 2020. [Medline] [CrossRef]
13. Cohen AS, and Calkins E. Electron microscopic observations on a fibrous component in amyloid of diverse origins. Nature. **183**: 1202–1203. 1959. [Medline] [CrossRef]
14. Lachmann HJ, Goodman HJB, Gilbertson JA, Gallimore JR, Sabin CA, Gillmore JD, and Hawkins PN. Natural history and outcome in systemic AA amyloidosis. N Engl J Med. **356**: 2361–2371. 2007. [Medline] [CrossRef]
15. Kamiie J, Sugahara G, Yoshimoto S, Aihara N, Mineshige T, Uetsuka K, and Shirota K. Identification of a unique amyloid sequence in AA amyloidosis of a pig associated with Streptococcus suis infection. Vet Pathol. **54**: 111–118. 2017. [Medline] [CrossRef]
16. Simons JP, Al-Shawi R, Ellmerich S, Speck I, Aslam S, Hutchinson WL, Mangione PP, Disterer P, Gilbertson JA, Hunt T, Millar DJ, Minogue S, Bodin K, Pepys MB, and Hawkins PN. Pathogenetic mechanisms of amyloid A amyloidosis. Proc Natl Acad Sci USA. **110**: 16115–16120. 2013. [Medline] [CrossRef]
17. Engelhardt JA, Gries CL, Long GG, and Lilly E. Incidence of spontaneous neoplastic and nonneoplastic lesions in Charles River CD-1 mice varies with breeding origin. Toxicol Pathol. **21**: 538–541. 1993. [Medline] [CrossRef]
18. Apreutese A, Levi M, Taylor I, Apreutese R, Mukaratirwa

S, and Mowat V. Causes of mortality and profile of spontaneous tumors in young CD-1 Mice. Toxicol Pathol. **50**: 776–786. 2022. [Medline] [CrossRef]
19. Hoffman JS, Ericsson LH, Eriksen N, Walsh KA, and Benditt EP. Murine tissue amyloid protein AA. NH2-terminal sequence identity with only one of two serum amyloid protein (ApoSAA) gene products. J Exp Med. **159**: 641–646. 1984. [Medline] [CrossRef]
20. Hébert L, and Gervais F. apo-SAA1/apo-SAA2 isotype ratios during casein- and amyloid-enhancing-factor-induced secondary amyloidosis in A/J and C57BL/6J mice mice. Scand J Immunol. **31**: 167–173. 1990. [Medline] [CrossRef]
21. Bansal A, Schmidt M, Rennegarbe M, Haupt C, Liberta F, Stecher S, Puscalau-Girtu I, Biedermann A, and Fändrich M. AA amyloid fibrils from diseased tissue are structurally different from in vitro formed SAA fibrils. Nat Commun. **12**: 1013. 2021. [Medline] [CrossRef]
22. Winter M, Tholey A, Krüger S, Schmidt H, and Röcken C. MALDI-mass spectrometry imaging identifies vitronectin as a common constituent of amyloid deposits. J Histochem Cytochem. **63**: 772–779. 2015. [Medline] [CrossRef]
23. Gaffney PM, Imai DM, Clifford DL, Ghassemian M, Sasik R, Chang AN, O'Brien TD, Coppinger J, Trejo M, Masliah E, Munson L, and Sigurdson C. Proteomic analysis of highly prevalent amyloid A amyloidosis endemic to endangered island foxes. PLoS One. **9**: e113765. 2014. [Medline] [CrossRef]
24. Inoue M, Miyazaki S, Kobayashi N, Kangawa A, and Murakami T. Pathological characterization of spontaneous AA amyloidosis in microminipigs. Toxicol Pathol. **51**: 257–263. 2023. [Medline] [CrossRef]
25. Zhang J, Guo W, Shi C, Zhang Y, Zhang C, Zhang L, Wang R, and Pan B. Copy number variations in serum amyloid A play a role in the determination of its individual baseline concentrations. Clin Chem. **64**: 402–404. 2018. [Medline] [CrossRef]
26. Hirouchi Y, Iwata H, Yamakawa S, Kato M, Kobayashi K, Yamamoto T, Inoue H, Enomoto M, Shiga A, and Koike Y. Historical data of neoplastic and non-neoplastic lesions in B6C3F1(C57BL/6CrSlc*C3H/HeSlc) mice. Toxicol Pathol. **7**: 153–177. 1994. [CrossRef]
27. Ward JM, Goodman DG, Squire RA, Chu KC, and Linhart MS. Neoplastic and nonneoplastic lesions in aging (C57BL/6N × C3H/HeN)F1 (B6C3F1) mice. J Natl Cancer Inst. **63**: 849–854. 1979. [Medline] [CrossRef]
28. Chandra M, and Frith CH. Spontaneous renal lesions in CD-1 and B6C3F1 mice. Exp Toxicol Pathol. **46**: 189–198. 1994. [Medline] [CrossRef]
29. Maronpot RR. Pathology of the Mouse, 1st ed. GA Boorman, and BW Gaul (eds). Cache River Press, Vienna. 1999.
30. Nonneoplastic Lesion Atlas. National Toxicology Program website: https://ntp.niehs.nih.gov/atlas/nnl/alimentary-system/stomach-glandular-stomach/Amyloid.
31. Schmitt R, Jacobi C, Susnik N, Broecker V, Haller H, and Melk A. Ageing mouse kidney—not always the SAME old story. Nephrol Dial Transplant. **24**: 3002–3005. 2009. [Medline] [CrossRef]
32. Pettan-Brewer C, and Treuting PM. Practical pathology of aging mice. Pathobiol Aging Age Relat Dis. **1**: 201. 2011. [Medline]